International Journal of Heat and Fluid Flow 117 (2026) 109990

Contents lists available at ScienceDirect

International Journal of Heat and Fluid Flow

journal homepage: www.elsevier.com/locate/ijhff

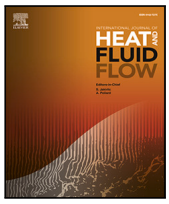

Fluid dynamic and thermal characterization of a turbulent shear layer

Francesco Scarano *, Emmanuel Jondeau, Édouard Salze

Laboratoire de Mécanique des Fluides et d'Acoustique, Ecole Centrale de Lyon, France
Institut National des Sciences Appliquées Lyon I, France
Université Claude Bernard Lyon I, Centre National de Recherche Scientifique, Université de Lyon, 36 av. Guy de Collongue, F-69134 Ecully, France

ARTICLE INFO

Keywords:
Mixing layer
Turbulent shear layer
Spectral Proper Orthogonal Decomposition
Hot wire anemometry
Cold wire anemometry
PIV

ABSTRACT

Planar particle image velocimetry (PIV) and hot-wire anemometry are used to study the turbulent shear layer that forms naturally from an initial laminar state due to velocity differences between a jet and its surrounding quiescent region. Spectral Proper Orthogonal Decomposition (SPOD) applied to PIV data reveals the presence of dominant large-scale coherent structures in the post-transition turbulent shear layer. These structures span the full thickness of the shear layer and account for approximately 30% of the total turbulent kinetic energy. They are associated with a Strouhal number of approximately 0.2, similar to that of Kelvin–Helmholtz instabilities typically observed in pre-transition regimes. This observation raises questions about the underlying growth mechanism: while the elongated spatial patterns are consistent with continuous structure growth, the Strouhal number suggests a behaviour more typical of pairing-dominated dynamics. The estimated structure spacing supports the hypothesis of a nearly constant spacing-to-thickness ratio. The thermal shear layer, characterized with CCA and CVA cold wires, was shown to exhibit self-similarity. The growth rate of the thermal shear layer differs from that of the velocity shear layer. New analytical formulations for universal non-dimensional profiles of mean temperature and standard deviation are presented.

1. Introduction

A fully developed plane turbulent shear layer is a self-sustaining turbulent flow in dynamic equilibrium, with its growth rate dependent solely on the velocity and density ratios of the free streams (Townsend, 1976). In the seminal work by Brown and Roshko (1974) it is reported that a mixing layer contains an organized processions of quasi-two-dimensional vortex-like large structures. These structures were assimilated with vortices produced by Kelvin–Helmholtz instability of the free-shear layer flow. As also reported by Michalke (1965), the vortices roll-up at a preferred frequency. Winant and Browand (1974) hypothesized that these vortices rotate and amalgamate in pairs leading to the linear growth of the fully developed turbulent mixing layer.

D'Ovidio and Coats (2013) characterized the growth and the interactions between the large organized structures in the pre and post-transition regime of a mixing layer at a variety of velocity and density ratios. They relied on flow visualization records of the complete field of the mixing layer development, obtained using Schlieren technique, to track the evolution of individual structures. They confirmed the growth by amalgamation in pre-transition mixing layer, they evaluated that the diameters of the structures changes in step afterwards an amalgamation. Conversely, in post-transition regime the mixing layer is dominated by a procession of spanwise coherent large structures. The large structures occupy individually the entire thickness of the mixing layer and expand steadily at a constant rate. The interactions between adjacent structures in the post-transition flow differ in nature from those in the pre-transition flow, arising as a result of the individual structures' growth rather than driving it. The growth of the individual structures is in turn responsible for the self-similar growth of the mixing layer thickness as whole by continuous entrainment of fluid. The results by D'Ovidio and Coats (2013) have been confirmed though three-dimensional large eddy simulations as reported in a follow-up paper (McMullan et al., 2015) where they replicated the laminar initial conditions of the wind tunnel experiment. They found that the large-scale structures in the post-transition mixing layer are intrinsically three-dimensional and if a two-dimensional simulation is performed, the hypothesis by Winant and Browand (1974) is valid even after the transition. McMullan et al. (2015) stated that the interactions between adjacent structures in the post-transition regime are driven by their ongoing growth, aiming to reduce the number of structures. This process helps maintaining a stable average spacing-to-thickness ratio, enabling the uninterrupted growth of the remaining structures.

The main goal of the current investigation is to characterize experimentally the velocity and thermal field of a mixing layer that develops

* Corresponding author.
E-mail address: fr.scarano@gmail.com (F. Scarano).

https://doi.org/10.1016/j.ijheatfluidflow.2025.109990
Received 7 February 2025; Received in revised form 12 June 2025; Accepted 17 July 2025
Available online 9 August 2025

naturally from initial laminar state due to the velocity differences between a jet and the quiescent region surrounding it. In particular, focus is given in verifying if, in the portion of the turbulent shear layer where self-similarity is verified, the turbulent shear layer is populated by large coherent structures. The studies by D'Ovidio and Coats (2013) and McMullan et al. (2015), in fact, show that the fully turbulent self-similar mixing layer maintains an organization which is similar to the pre-transition mixing layer. To confirm this hypothesis, the dynamics of the turbulent shear layer is studied relying on Spectral Proper Orthogonal Decomposition (SPOD) (Schmidt and Colonius, 2020) applied to Particle Image Velocimetry (PIV) data. PIV data should provide more quantitative results about the coherent structures in post-transition regime compared with flow visualization data obtained by D'Ovidio and Coats (2013).

In the second part of the paper the thermal shear layer that develops due to the different temperature between the core of the jet and its surrounding is characterized with cold wire anemometry. Only a few studies, such as Ferchichi and Tavoularis (1992), have investigated the self-similar development of a thermal turbulent shear layer. However, a comprehensive characterization using state-of-the-art temperature measurement techniques capable of high-frequency acquisition is still lacking in the literature. The objective is to provide self-similarity laws for the temperature statistics, this can evidence analogies with the velocity field. A complete description of thermal self similarity is indeed not detailed in the literature.

2. Experimental apparatus

The experiments are carried out in the anechoic open jet wind tunnel at the Laboratoire de Mécanique des Fluides et d'Acoustique (LMFA), located at the École Centrale de Lyon. The jet is outfitted with an inlet that has a contraction ratio of 1.25, terminating in a square exit with a side length of 0.5 m. The setup allows a maximum achievable speed of approximately 80 m/s.

Particular care was taken in choosing the measurement location. To minimize the influence of three-dimensional effects originating from the corner regions of the square nozzle, the PIV measurements were conducted at the vertical mid-plane, at half the nozzle height. This central positioning reduces the risk of contamination from top and bottom shear layers, which would be more pronounced near the edges. Similar to prior experimental and numerical studies (Candel et al., 1976a; Bennaceur, 2017; Bell and Mehta, 1990) on free shear layers, we selected the region between 0.3 m and 0.7 m downstream of the nozzle as our domain of investigation. This region allows to capture the self-similar development and the representative dynamics of the turbulent shear layer.

To measure the velocity field, two techniques are used: particle image velocimetry (PIV) and constant temperature hot wire anemometry (CTA). A cold wire probe is employed to investigate the thermal shear layer. The cold wire anemometer used is either a constant current anemometer (CCA) or a constant voltage anemometer (CVA). The measurements from both the hot and cold wires are synchronized. The separation between the two wires is roughly 2 mm, ensuring that temperature readings are taken at the same location as the velocity measurements. Additional measurements with isolated probes confirmed that both aerodynamic and thermal interactions between the wires are negligible. A thermocouple is mounted on the cold wire support to serve as a reference for the mean temperature. This thermocouple allows for the determination of the mean temperature when the CVA cold wire is in use, as the CVA is capable of measuring only temperature fluctuations.

Planar PIV measurements are conducted at 35 m/s and 55 m/s during a separate experimental campaign. The measurement plane is horizontal (xy-plane), with the PIV plane centred 500 mm downstream of the nozzle exit as shown in Fig. 1. The shear layer is examined using both hot and cold wire probes at 55 m/s at three streamwise positions: 300, 500, and 700 mm downstream of the exit section. The two probes are traversed across the shear layer in the transverse direction, y, with a minimum displacement of 0.01 mm. To assess the self-similarity of the shear layer in relation to variations in free-stream velocity, profiles at 35 m/s and 75 m/s are obtained at a streamwise position of $x = 500$ mm. The signals from both the hot and cold wire probes are recorded using a National Instruments PXI-4472 data acquisition system. The sampling frequency is set at 104 kHz (maximum sampling rate of the DAQ card), with a sampling duration of 20 s per y-position, and 90 s for spectral measurements.

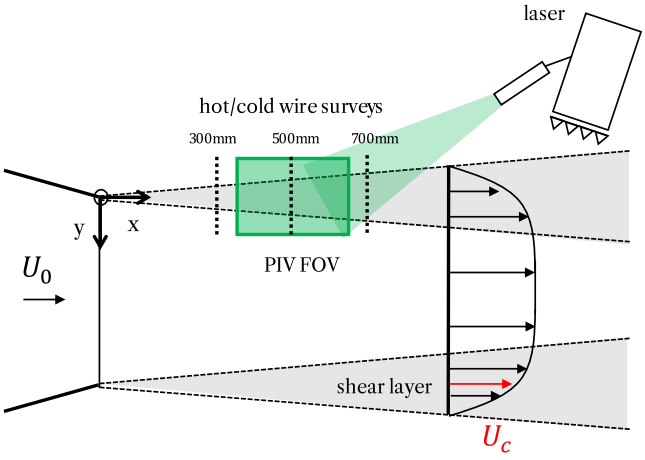

Fig. 1. Sketch of the experimental setup.

2.1. Particle image velocimetry

A double-pulsed Continuum Mesa PIV laser is employed to illuminate the particles. Two smoke generators are utilized in the experiments: one for seeding the core of the jet and the other for seeding the anechoic chamber, ensuring an adequate particle density throughout the shear layer region. To maintain the particle image size between 2 and 4 pixels and minimize peak-locking effects, the particle images are intentionally defocused, as recommended by Michaelis et al. (2016). A Phantom VEO1310L 12-bit CMOS camera, equipped with a 60 mm f/2.8 Micro Nikkor lens, is used for imaging. Lavision DAVIS 10.2 software is responsible for the calibration, synchronization, laser control, and image acquisition, with the acquisition frequency set to 5 kHz. Each measurement run consists of 4900 image pairs collected over a duration of 0.98 s. Approximately 20 runs are conducted to ensure sufficient statistical convergence, thereby resolving the most significant flow features. This corresponds to approximately 920 and 1480 large scale structure passage times for the two velocities. The acquired samples are processed using the 2D2C cross-correlation PIV algorithm in DAVIS 10.2. The interrogation window size was iteratively changed passing from 64 × 64 pixel to 8 × 8 with an overlap of 50%; this leads to a vector spacing of $\Delta x = \Delta y = 0.665$ mm and 34 200 vectors. The field of view (FOV) is 158 mm × 212 mm ($2.2\delta_\omega \times 1.6\delta_\omega$, where δ_ω is the vorticity thickness). The uncertainty in the instantaneous velocity measurements is estimated following the approach described by Sciacchitano (2019). An uncertainty of approximately 4% is observed in the high-speed region, increasing to over 5% in the low-speed region of the shear layer. This increase is due to the reduced particle displacement in the low-speed region, which affects the accuracy of the PIV cross-correlation algorithm.

2.2. Hot wire: constant temperature anemometer (CTA)

A Dantec gold-plated hot wire probe (model 55P01) with a length of 1.25 mm and a diameter of 5 μm is employed to conduct velocity

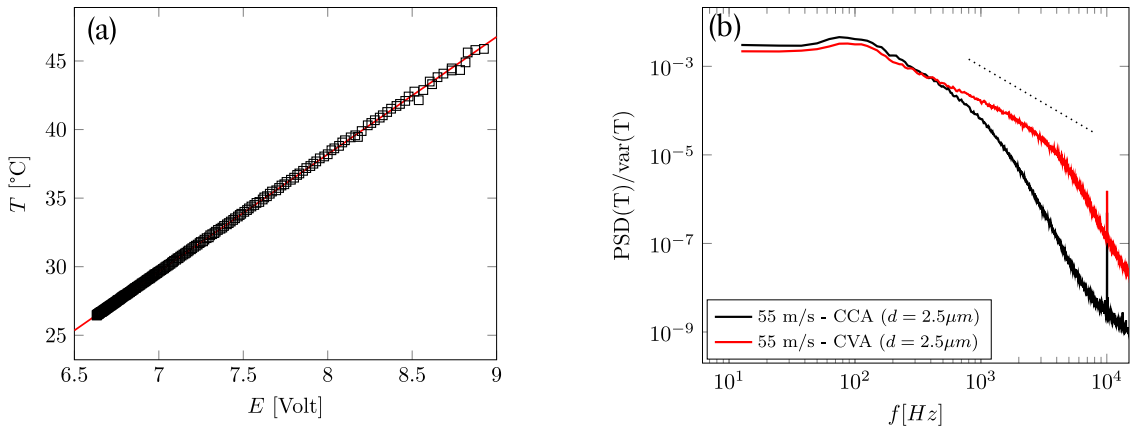

Fig. 2. (a) Constant current anemometer cold wire calibration curve, (b) temperature spectra at the peak of the σ_T profile, $x = 0.5$ m and $U_0 = 55$ m/s, comparison CCA and CVA.

surveys within the shear layer. The wire is conditioned and operated through a Dantec Streamline Pro CTA Module 90C10. An overheat ratio of 0.8 is applied. The wire's temperature after conditioning is determined by measuring its resistance, yielding a value of $T_w = 238°$ C. The system's frequency response, determined with a square wave test, is 85 kHz, and is evaluated at the maximum test velocity. Velocity calibration is carried out *in situ* within the jet core using a pitot tube. The calibration curve is derived with a fourth-order polynomial fit, as described by Perry (1982). In accordance with the methodology outlined in Scarano et al. (2024), the hot wire signal is corrected to account for local temperature drift within the shear layer.

The acquisition time for each hot wire measurement point is 20 s when used for the velocity profiles, and 60 s for measurements used to compute spectra and autocorrelation. The 60 s duration corresponds to approximately 2760, 4512 and 5520 large-structure passage times, respectively, for the three freestream velocities considered.

2.3. Cold wire: constant current anemometer (CCA) and constant voltage anemometer (CVA)

A cold wire is a fine-wire sensor operated at a very low overheat ratio, enabling the measurement of time-varying temperature fluctuations (Berson et al., 2010). Cold wires can be operated by constant current anemometers (CCA) or constant voltage anemometers (CVA), with the latter offering thermal inertia compensation through hardware corrections, resulting in improved frequency response. The differing frequency responses of the two cold wire configurations are demonstrated by comparing the temperature spectra within the shear layer, as shown in Fig. 2(b). The cut-off frequency for the CCA setup is approximately 900 Hz, whereas it increases to 3000 Hz for the CVA. For the CVA system, only temperature fluctuations can be measured directly, necessitating the use of a type K thermocouple to determine both the mean and fluctuating temperature, as outlined in Cleve et al. (2017). For more detailed information on the CCA and CVA systems, the reader is referred to Tropea et al. (2007).

In the present setup, the cold wire is a modified in-house Dantec 55P11 with a length of 1.25 mm and a diameter of 2.5 μ m, made from tungsten. It operates as either a CCA or CVA, depending on the specific case. The CCA is powered with a current of 0.1 mA through a Dantec Streamline temperature module 90C20, while the CVA utilizes a Tao Systems CVA model 5003 with an input voltage of 8.03 mV across the wire circuit. Both the current and voltage are calibrated using a multimeter prior to the measurements. The calibration of the CCA system is conducted in a separate calibration oven at zero free-stream velocity, where the temperature is varied within the relevant range for the current study. The calibration curve for the CCA cold wire, shown in Fig. 2(a), establishes a direct relationship between the output voltage and the flow temperature. For the CVA, the calibration follows the procedure outlined by Mohammed-Taifour et al. (2015) and Mercier et al. (2019), which automatically compensates for thermal inertia to obtain accurate temperature fluctuations. The acquisition time is analogous to the hot wire anemometry measurements.

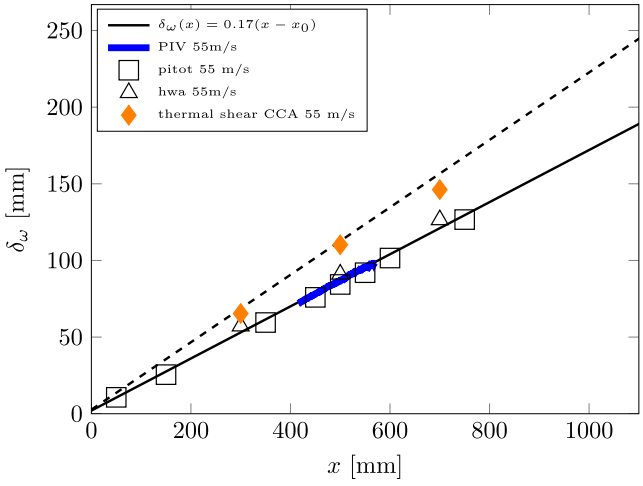

Fig. 3. Streamwise evolution of the vorticity thickness, different corrections method and thermal shear layer measurements measured with the CCA. (For interpretation of the references to colour in this figure legend, the reader is referred to the web version of this article.)

3. Results

3.1. Velocity statistics and self-similarity of the velocity field

A free shear layer develops when two initially separated uniform velocities U_a and U_b, where in general $U_a > U_b$, interact forming a mixing region. It is possible to define the convective velocity U_c as

$$U_c = (U_a + U_b)/2 \tag{1}$$

and the velocity ratio $R = (U_a - U_b)/(2U_c)$. In the current setup the two velocities U_a and U_b are equal to U_0, velocity of the core of the jet, and 0. This leads to a definition of the convective velocity, $U_c = U_0/2$ and the velocity ratio in the current case is equal to one. The vorticity thickness is defined as

$$\delta_\omega(x) = \frac{U_a - U_b}{\left(\frac{\partial U(x)}{\partial y}\right)_{\max}} \tag{2}$$

where y is the spanwise coordinate that traverses the turbulent shear layer.

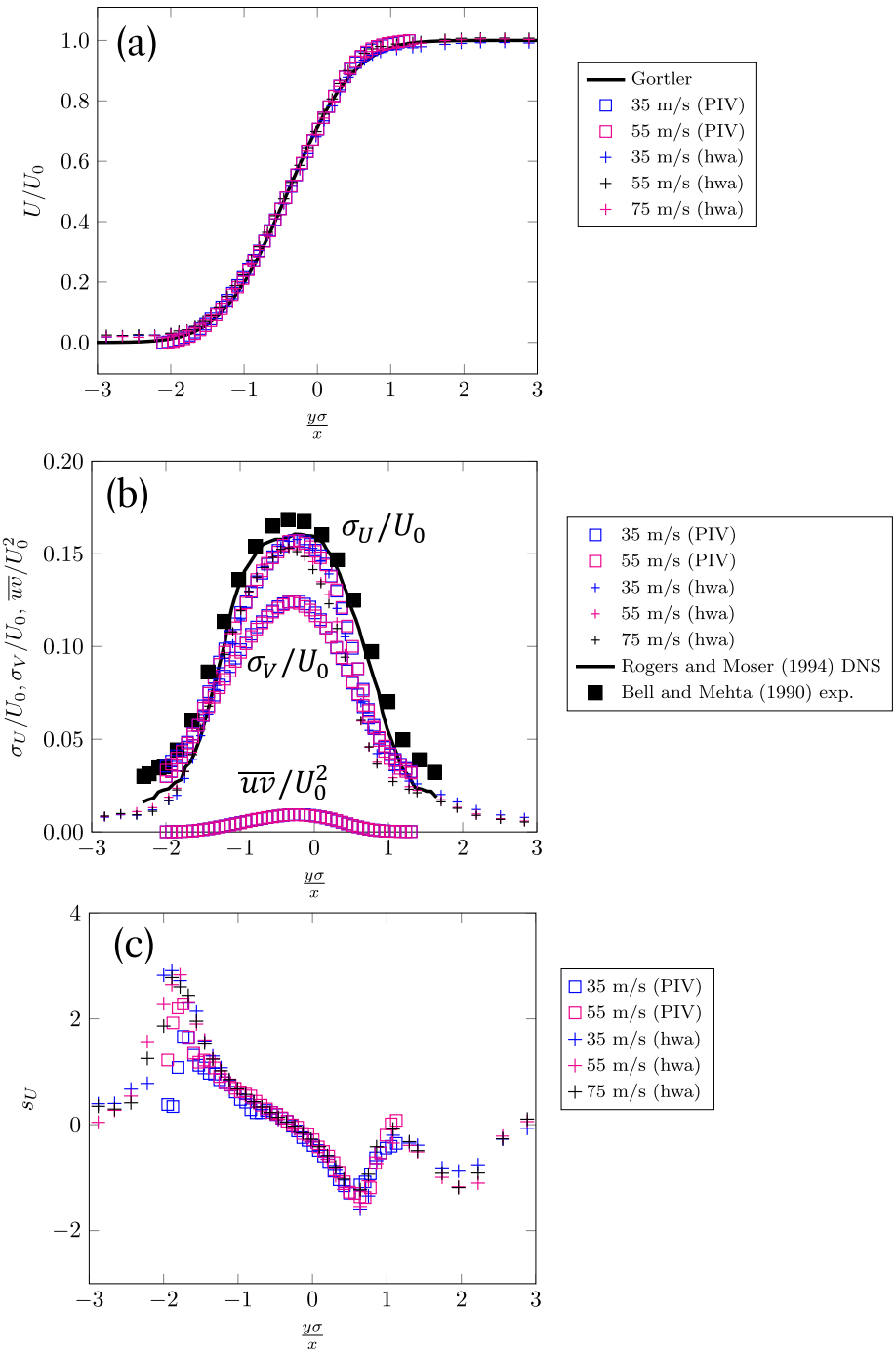

Fig. 4. Non dimensional mean velocity U/U_0 (a), standard deviation σ_U/U_0, σ_V/U_0 and Reynolds shear stress (b) and skewness profiles (c). Effect of the free-stream condition U_0. Comparison PIV and hot wire anemometry results with theoretical profile by Gortler (1942) and experimental and numerical data by Rogers and Moser (1994) and Bell and Mehta (1990).

The evolution of the turbulent shear layer is self-similar downstream a certain streamwise coordinate. For a self-similar turbulent shear layer, the vorticity thickness can be expressed as function of the streamwise coordinate following the relation proposed by Gortler (1942)

$$\delta_\omega(x) \cong 4\frac{x - x_0}{\sigma\sqrt{2\pi}} \tag{3}$$

where σ is called spreading parameter and varies between 9 and 11 and x_0 is the streamwise coordinate where the self-similarity starts. Another expression is found experimentally by Candel et al. (1976b)

$$\delta_\omega(x) \cong 0.17(x - x_0). \tag{4}$$

These relations highlight that when the shear layer is self-similar the growth of the shear layer only depends on the streamwise coordinate.

According to Brown and Roshko (1974) the spreading of the shear layer thickness only depends on the velocity and on the density ratio. In our case, the density variation due to temperature differences is moderate, with an Atwood number ranging from 0.016 to 0.032 depending on the thermal conditions. The velocity ratio is fixed at $R = 1$ for all configurations. For this reason for the three velocities the same growth rate is expected. The streamwise evolution of the vorticity thickness is reported inFig. 3 along with the thermal vorticity thickness that will be discussed hereafter. Hot wire anemometry, PIV measurements and additional pitot surveys are reported to cover a larger portion of

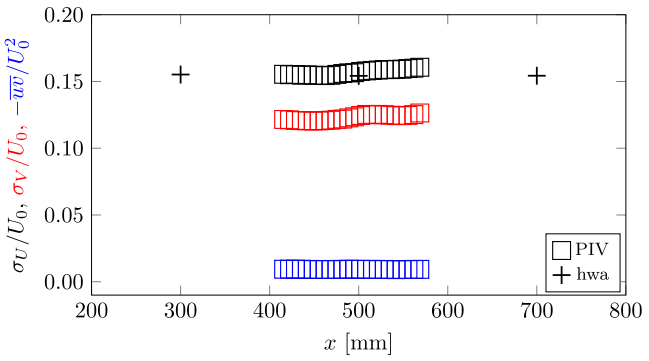

Fig. 5. Plateau of the shear stresses peaks along the streamwise direction, comparison PIV and hot wire anemometry results.

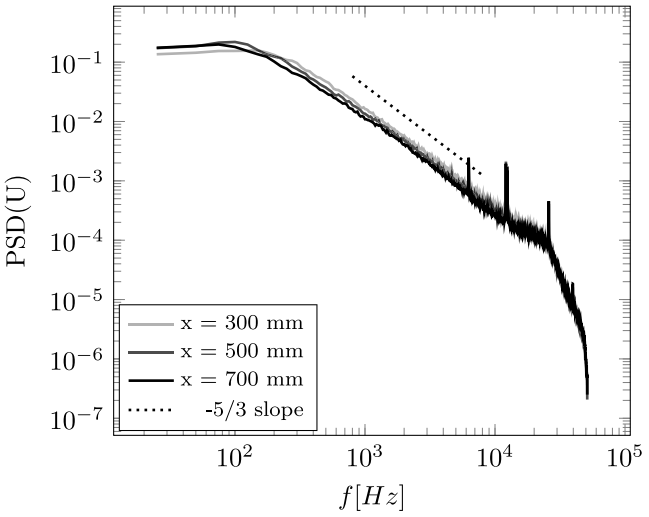

Fig. 6. Streamwise velocity spectrum at 55 m/s obtained in correspondence of the σ_U/U_0 peak at three streamwise positions.

the shear layer evolution. The results show a perfect linear growth in agreement with the semi-empirical relation reported by Candel et al. (1976a) using $x_0 = 0.1$ m.

At the measurement location of $x = 0.5$ m, the Reynolds number based on the vorticity thickness, Re_{δ_ω}, is equal to 1.9×10^5, 3.0×10^5, and 4.1×10^5 for the three tested free-stream velocities. These values are sufficiently high to indicate that the shear layer has undergone transition and is fully turbulent.

Bell and Mehta (1990) underlined that the linear growth of the shear layer thickness is a necessary but not sufficient condition for the achievement of self-similarity. The three conditions in order to achieve self-similarity are: linear growth of the shear layer thickness, collapse of mean and turbulence profiles when plotted using reduced quantities, values of the shear stresses that reach an asymptotic values in the streamwise direction, x.

According to Gortler (1942) the dimensionless mean velocity profiles when the turbulent shear layer is self-similar can be approximated by

$$\frac{U(\eta)}{U_0} = \frac{1}{2}[1 + \mathrm{erf}(\eta + \eta_0)] \tag{5}$$

where η_0 is the expansion of the potential core and erf() is the Gauss error function. The similarity variable η is function of the streamwise coordinate

$$\eta = \sigma \frac{y}{x}. \tag{6}$$

Th values of η_0 and σ can be obtained by fitting the experimental profile with the theoretical curve. In the current investigation the value of the spreading parameter is equal to 11 and the expansion of the potential core is 0.4; these values are not dissimilar with respect to the ones reported in the literature.

The self-similarity of the normalized mean streamwise velocity, U, standard deviation of the two velocity coordinates, σ_U and σ_V, Reynolds shear stress $\overline{uv}$ and skewness, s_U, at $x = 500$ mm when changing the free-stream velocity U_0 are reported in Fig. 4. The collapse of the profiles when using both measurement technique is excellent. The standard deviation of the streamwise velocity profiles is compared with Rogers and Moser (1994) and Bell and Mehta (1990) again showing a good match.

The plateau of the normalized streamwise and spanwise velocity variances, as well as the Reynolds shear stress peak, along the streamwise direction is shown in Fig. 5. The results are based on PIV measurements spanning the region around $x = 0.5$ m. A nearly constant value of $\overline{uv}$, σ_U, and σ_V is observed in this range. Additional hot-wire anemometry measurements conducted at $x = 0.3$ m and $x = 0.7$ m confirm the constancy of σ_U, supporting the onset of self-similarity upstream of the PIV field of view.

Finally the streamwise velocity spectrum, obtained in correspondence of the peak of σ_U, is reported in Fig. 6 at 55 m/s for three streamwise coordinate. The slope of the inertial sub-range further corroborates that the turbulence is well developed and canonical at every streamwise coordinate of the shear layer investigated.

To verify the two-dimensionality of the flow at the measurement location, we conducted complementary hot-wire measurements across different vertical positions in the vicinity of the mid-height of the nozzle (not shown here) and observed negligible variation in key turbulence statistics, indicating that the shear layer at $x = 0.5$ m is fully developed and not strongly influenced by nearby shear layers. This is further supported by the observation of self-similarity in both the velocity and temperature profiles (see Section 3.4) at multiple streamwise positions, which is a hallmark of canonical shear layer behaviour. Beyond $x = 0.7$ m, however, the variation in turbulence statistics at various vertical positions became significant, indicating the merging of shear layers from multiple nozzle edges and the emergence of stronger three-dimensional effects.

By verifying the self-similarity and turbulent spectra we thus verified that the mixing layer is in the post-transition regime. The following step will be to verify the coherent structures that populate the turbulent shear layer.

3.2. Spectral proper orthogonal decomposition

To investigate the nature of the physical mechanism that dominates the shear layer dynamics, the spectral proper orthogonal decomposition (SPOD) analysis is performed on the PIV data-set. SPOD allows to extract from statistically stationary data, as the PIV data-set of the current investigation, an optimal orthogonal basis where a high fraction of the total energy is retained in a few modes that express coherence both in time and space (Schmidt and Colonius, 2020).

The SPOD is performed on both the streamwise, U, and spanwise, V, coordinate of the flow. For the SPOD analysis, the Matlab routines reported by Towne et al. (2018) are used. Being the Nyquist frequency of 2.5 kHz the data sample are well resolved in time. Each data-set (RUN) is divided in 37 Hamming windows of 256 snapshots with 50% overlap; changing the window size does not influence the results. The SPOD spectra are reported in Fig. 7(a) at 35 m/s and Fig. 7(b) 55 m/s where on the abscissa it is reported the Strouhal number calculated with the vorticity thickness. The low rank behaviour of the first mode is illustrated by representing in grey the ten most energetic modes. The first mode (thicker line) for both the velocity coordinates contains almost 30% of the total turbulent kinetic energy for both free-stream

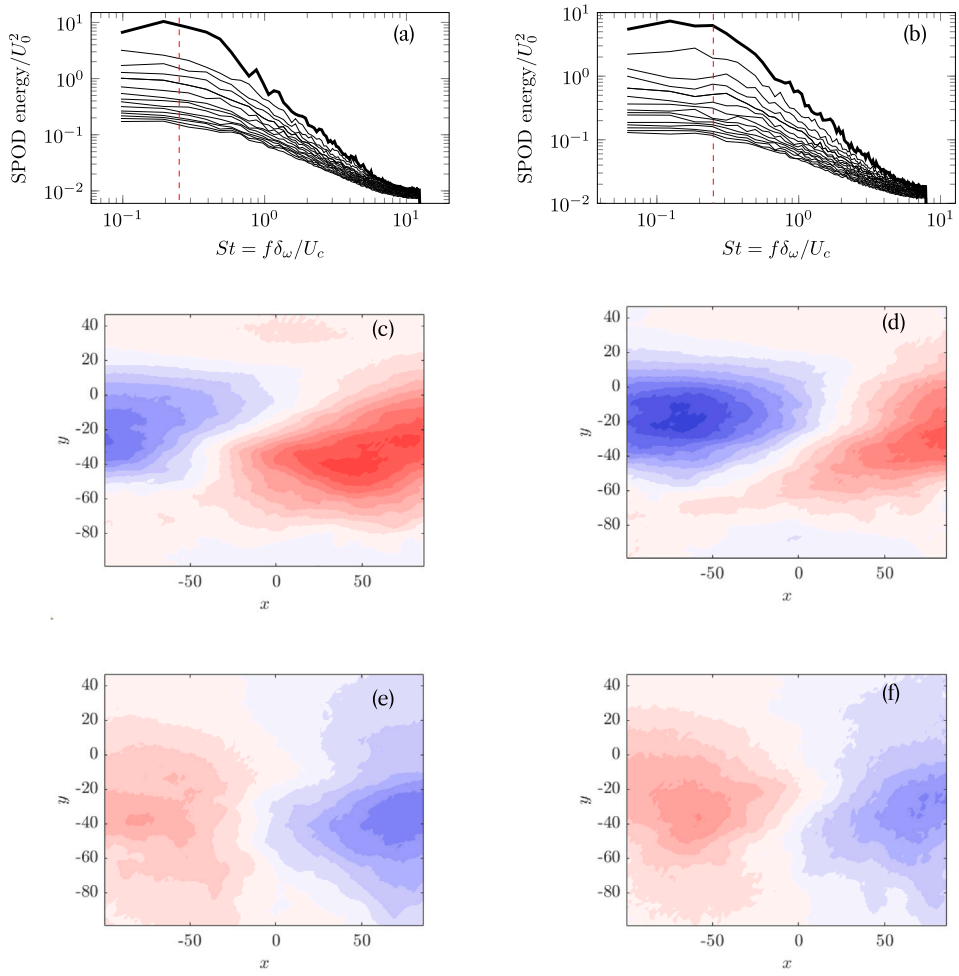

Fig. 7. SPOD results, left column at U_0 = 35 m/s and right column at 55 m/s; (a) and (b) SPOD spectra, the red dashed line is the Strouhal number of 0.25, (c) and (d) first mode at the Strouhal number of 0.25 for the streamwise velocity, U and (e) (f) transverse velocity, V. Contours axis are centred at the PIV field of view plane ($x = 0$ located 500 mm downstream of the nozzle, $y = 0$ is 30 mm outwards of the nozzle edge).

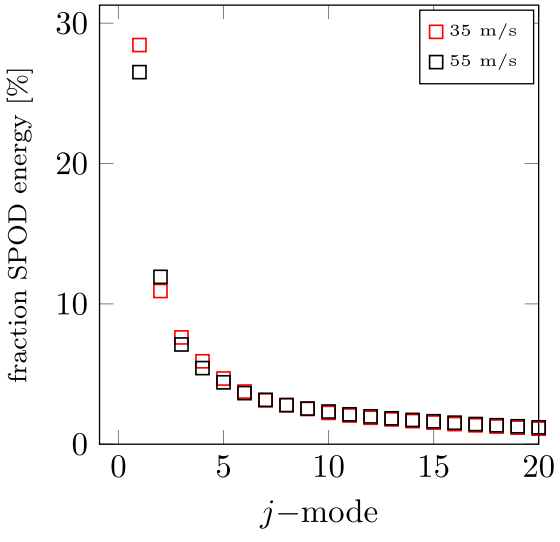

Fig. 8. Fractional energy content associated with each SPOD mode.

velocities as can be depicted from Fig. 8. The results reported herein are found to not vary from one RUN to another.

The spectra of the most energetic mode for both velocities are dominated by a hump which is centred around a low frequency which corresponds to a Strouhal number of approximately 0.2. This Strouhal number is not dissimilar to the reduced frequency of the passage of large scale, quasi-two dimensional structures in mixing layers (0.25–0.27) obtained by Browand and Troutt (1985). According to Brown and Roshko (1974) these structures are similar to the two dimensional roller forming due to the instability of a laminar shear layer in the pre-transition regime. As stated by Brown and Roshko (1974) the scales, and thus the reduced frequencies, associated with the coherent structures are associated with a broad hump in the velocity fluctuation energy spectrum It is remarkable that this reduced frequency, typical of the Kelvin Helmholtz instability, persists in the post-transition phases. This result partially contradict the results proposed by D'Ovidio and Coats (2013). However a modal decomposition was not performed in their analysis as the results were based on flow visualization.

The modes of the streamwise coordinate, associated with this reduced frequency, are reported in Fig. 7(c) and (d) for 35 and 55 m/s respectively. While the full streamwise extent of individual structures may not be entirely captured within the PIV field of view, the SPOD results reveal elongated spatial patterns that extend across the entire transverse width of the shear layer. The modes of the V velocity coordinate consist in an alternated and oriented pattern of transverse velocity. It is remarkable that the modes for the two velocities are identical suggesting that for both free-stream conditions the turbulent shear layer has reached the same self-preserving equilibrium state.

The SPOD analysis confirms the presence of dominant large-scale structures, consistent with findings from previous studies of turbulent shear layers. In agreement with D'Ovidio and Coats (2013) and McMullan et al. (2015), the structures educed from SPOD occupy the entire transverse extent of the shear layer. The spatial pattern resembles what McMullan et al. (2015) describe as a *flow cell*—a structure that

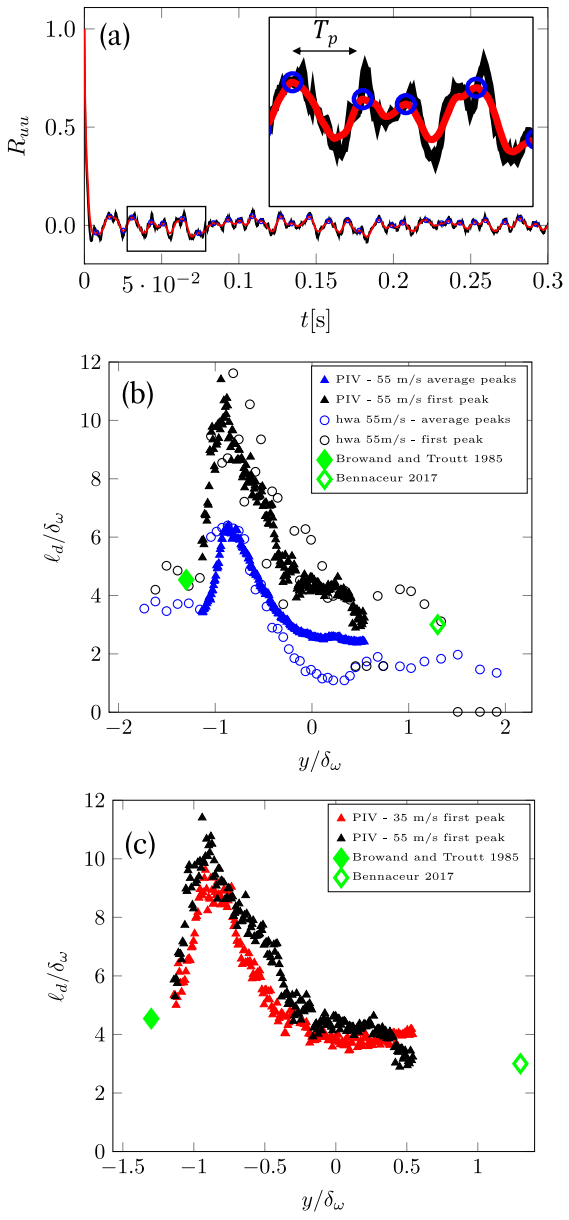

Fig. 9. (a) Autocorrelation function R_{uu} $x = 0$ on the low speed region, smoothed curve reported in red, in blue the identification of the maxima, (b) spacing calculated using the first peak (Browand and Troutt, 1985) and the average spacing between the peaks (Bennaceur, 2017) and further comparison with hwa data (c) comparison between 35 and 55 m/s. (For interpretation of the references to colour in this figure legend, the reader is referred to the web version of this article.)

contributes to continuous fluid entrainment and shear layer growth in the post-mixing transition regime.

However, the interpretation of SPOD modes requires caution. While our results are consistent with a continuous-growth mechanism, as opposed to the classical merger-dominated evolution, this distinction remains the subject of ongoing debate (Carlier and Sodjavi, 2016; Gautam et al., 2024). A central question raised in recent literature is why post-transition shear layers, if governed by a different growth mechanism, exhibit similar self-similar growth rates and Strouhal numbers to pre-transition (Kelvin–Helmholtz-dominated) layers, as also observed in 2D simulations (Suryanarayanan and Narasimha, 2017). Our measurements yield a dominant Strouhal number of approximately 0.2, comparable to those typically associated with pre-transition shear layers, thus reinforcing this ambiguity.

Moreover, it is important to consider that SPOD modes represent energy-weighted averages over time. In a scenario where coherent structures grow via vortex pairing, their instantaneous vertical positions may vary between realizations. The resulting SPOD modes would then reflect an ensemble-averaged structure that spans the shear layer in the vertical direction and appears centred, even though the instantaneous structures may fluctuate in position due to pairing events or local asymmetries. In other words, the apparent symmetry and spatial extent of the SPOD mode may be a consequence of temporal averaging rather than a direct representation of individual coherent structures. Such averaging may produce modal shapes similar to those shown in Fig. 7, regardless of whether the underlying mechanism is pairing or continuously-driven.

Finally, we note that due to the limited streamwise extent of the PIV field of view ($L < 3\delta_\omega$), it is not possible to directly track the streamwise growth of the dominant structures. For this reason, while the SPOD results support the continuous-growth hypothesis qualitatively they could also be compatible with a merger-driven evolution. We refrain from making definitive claims and instead present this analysis as contributing experimental evidence to the ongoing discussion on post-transition shear layer dynamics.

3.3. Spacing between the large structures

Having observed that the dominant SPOD structures span the entire transverse extent of the shear layer, consistent with those reported by D'Ovidio and Coats (2013), we next focus on evaluating the spacing between these structures. As hypothesized by the D'Ovidio and Coats (2013) and McMullan et al. (2015) the interactions between neighbouring structures in the post-transition regime resulted from their ongoing growth and served to periodically reduce the number of structures. This ensured a consistent average spacing-to-thickness ratio, allowing the remaining structures to grow without obstruction.

The spacing between the large structures was firstly calculated by Brown and Roshko (1974) from flow visualization; the value reported was around 3.2 times the vorticity thickness. The results have been recently confirmed by Bennaceur (2017) who, relying on numerical simulations, found an average large structure spacing between 3 and 3.2 times the vorticity thickness. However Browand and Troutt (1985) report a relation that links the mean spacing with the velocity ratio R

$$\ell_p = 0.54R + 4.0 \tag{7}$$

that for the current case gives a value of 4.45.

Browand and Troutt (1985) and Bennaceur (2017) computed the spacing between the large structures by computing the time interval between the passage of two consecutive structures, T_p, and multiplying it by the convection velocity: $\ell_p = T_p U_c$. The passage time is calculated starting from the autocorrelation function R_{uu} of a point located at a fixed streamwise position and at a transverse position located at the edge of the shear layer where the velocity signal is more sensitive to large structures. According to Browand and Troutt (1985) the position at $y = 1.3\delta_\omega$ on the low-speed side is the most appropriate because the signal is only sensitive to large scale vortices and it is not contaminated by the small scale vortices of the high-speed side of the mixing layer which are predominant towards the core of the jet. (Browand and Troutt, 1985) highlighted that even a small variability in the choice of the transverse location leads to an erroneous evaluation of the spacing between the structures. Bennaceur (2017) calculates the large vortices spacing at a similar transverse location but on the high speed side, this could explain the discrepancies in his results. The main difference between the two studies, however, relies in the definition of the passage time T_p from the autocorrelation function. The autocorrelation function has a shape that is quasi-periodic with relative peaks as high as 0.2. According to Bennaceur (2017) T_p can be calculated as the average interval between two maxima in the R_{uu} (averaged on the entire signal)

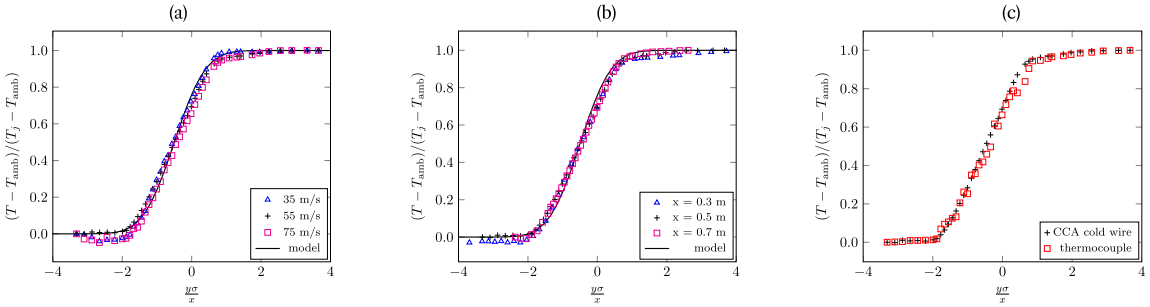

Fig. 10. Self similarity of the mean temperature profile of the shear layer, (a) effect of the velocity at $x = 0.5\,\mathrm{m}$ and (b) effect of the streamwise position for $U_0 = 55\,\mathrm{m/s}$, (c) comparison CCA cold wire and thermocouple for $U_0 = 55\,\mathrm{m/s}$ at $x = 0.5\,\mathrm{m}$.

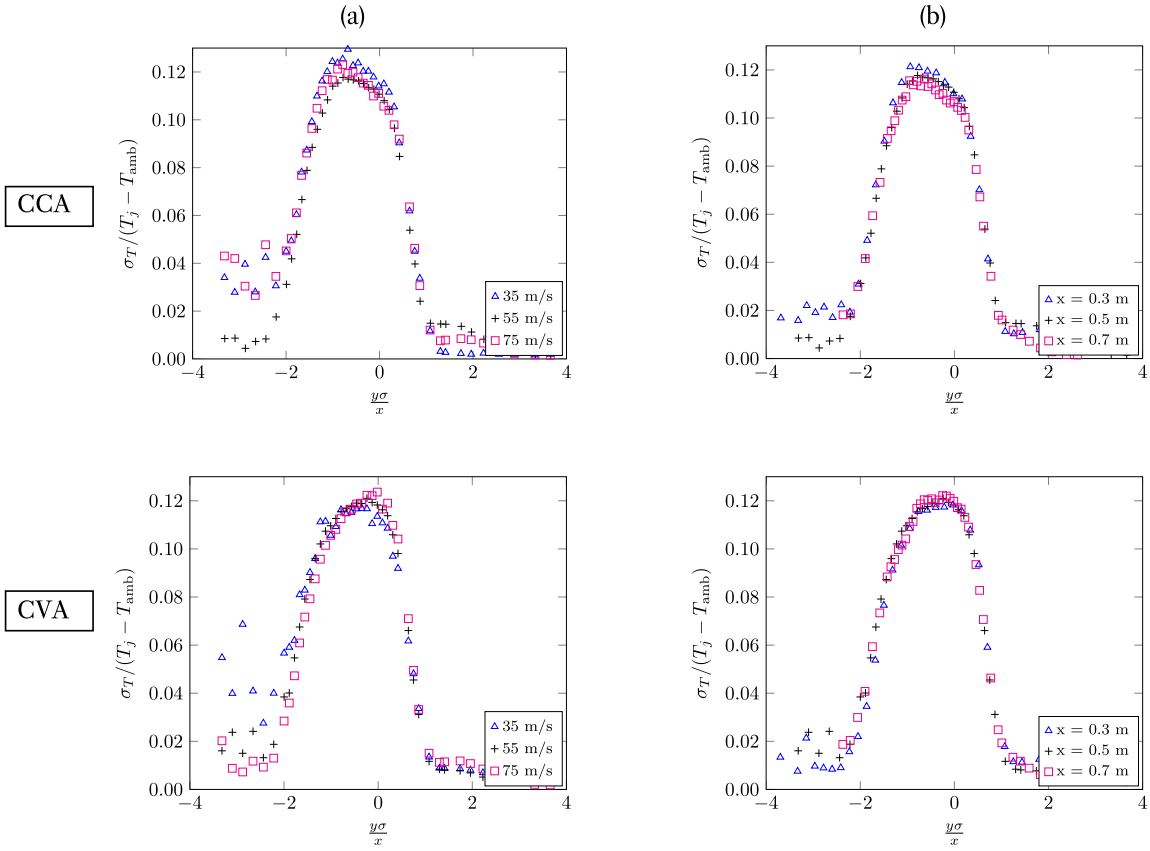

Fig. 11. Self similarity of the non dimensional temperature standard deviation profile of the shear layer, column (a) effect of the velocity at $x = 0.5\,\mathrm{m}$ and column (b) effect of the streamwise position for $U_0 = 55\,\mathrm{m/s}$, CCA and CVA cold wire results.

whereas in the paper by Browand and Troutt (1985) T_p is the time interval to the first peak of the autocorrelation function.

The autocorrelation at the edge of the shear layer is reported in Fig. 9(a). The autocorrelation is smoothed (red curve on the figure) with a moving average function to better identify the maxima (the blue circles in the figure). In Fig. 9(b) the two methods to define the passage time T_p are compared for 55 m/s. Additional hot wire measurements are performed at the transverse position prescribed by Browand and Troutt (1985), which is outside the PIV field of view. As depicted in Fig. 9(b) the shape of the spacing profile is similar for the two methods. The spacing between the structures is underestimated if the average T_p of the signal is considered, this because the autocorrelation function asymptotically tends to zero as the time increases and the uncertainty in the identification of the local maxima increases. The current results for both 35 and 55 m/s match quite well the ones reported in the literature following the two different methods. In particular, the value obtained using the first peak as passage time (Browand and Troutt, 1985) corresponds approximately to a scaled spacing of $4.3\delta_\omega$ which is in perfect agreement with respect to Eq. (7).

Interestingly, the passage time corresponds to a Strouhal number approximately equal to 0.23 which is in decent agreement with the reduced frequency which corresponds to the most energetic SPOD mode. This suggests that large structures, educed from SPOD, have a characteristic separation spacing that scales with the vorticity thickness, as suggested by D'Ovidio and Coats (2013) and McMullan et al. (2015), and their passage keeps the same reduced frequency has a Kelvin Helmholtz instability typical of the pre-transition regime.

3.4. Temperature statistics and self-similarity of the thermal shear layer

The work by Ferchichi and Tavoularis (1992) suggested that the thermal shear layer evolves self-similarly as the velocity shear layer.

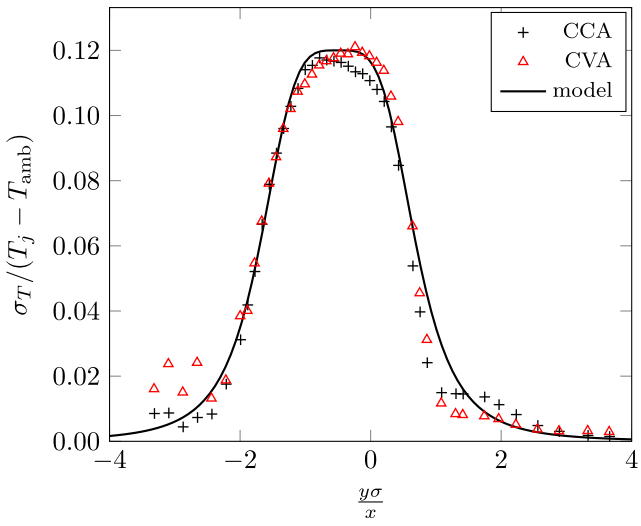

Fig. 12. Non dimensional temperature standard deviation profile, comparison CCA and CVA cold wire results for $U_0 = 55\,\mathrm{m/s}$ at $x = 0.5\,\mathrm{m}$, solid line analytical model.

In the current investigation the temperature mean profiles are acquired with the CCA and the thermocouple while the statistics can be computed from the CCA and the CVA.

In the Fig. 10 the mean temperature profiles obtained with the CCA are reported. The reduced transverse coordinate, $\sigma y/x$, is obtained with the same spreading parameter obtained for the velocity shear layer, namely $\sigma = 11$. The temperature profiles are normalized by subtracting the ambient temperature, T_{amb} and by dividing the value by the temperature difference between the core of the jet, T_j and the ambient temperature. In Fig. 10(a) (b) the effect of the variation of the free-stream velocity and the streamwise position are reported. It is clear that, similarly to the mean velocity profile, if the aforementioned normalization is applied, the mean thermal shear layer is self similar following an error function in analogy with the velocity shear layer

$$\frac{T(\eta) - T_{amb}}{T_j - T_{amb}} = \frac{1}{2}[1 + \mathrm{erf}(\eta + \eta_0)] \tag{8}$$

where η_0 is the expansion of the core of the thermal shear layer and it is found to be equal to 0.5, larger than the value obtained for the velocity shear layer. Moderate variation in the temperature that leads to a local deviation from the error function is found in the low speed side (low temperature side). This is attributed to natural convection and flow recirculation in the test section. In Fig. 10(c) the comparison between the simultaneous measurements obtained with the CCA and the thermocouple are presented. Despite a systematic offset between the two instruments, when normalized, the profiles collapse on each other, this can be seen as a further confirmation of the correctness of the normalization that differs from the one proposed by Ferchichi and Tavoularis (1992).

The thermal vorticity thickness, δ_{ω_T}, can be defined in analogy with the vorticity thickness

$$\delta_{\omega_T}(x) = \frac{T_j - T_{amb}}{\left(\frac{\partial T(x)}{\partial y}\right)_{max}}. \tag{9}$$

The streamwise evolution of the thermal vorticity thickness is reported in Fig. 3 in orange. As for the velocity shear, the thermal shear grows linearly but with a slope that is larger than the velocity counterpart. The experimental fit, in fact evidences a slope about 0.22 while it is approximately equal to 0.17 for the velocity shear layer in agreement with Candel et al. (1976a). The ratio of the slopes is approximately equal to 0.7 meaning that the thermal shear layer grows faster than the velocity shear layer.

The temperature standard deviation profile, σ_T, is illustrated in Fig. 11; the results are obtained with the CCA and with the CVA. The collapse of the profile is evident especially for the CVA results, while the CCA results show some differences in the normalized peak value that, for all the cases, is approximately equal to 0.12. Even in this case the normalization is obtained using the temperature differences between the core of the jet and the ambient temperature.

In Fig. 12 CVA and CCA measurements are compared for $U_0 = 55\,\mathrm{m/s}$ at $x = 0.5\,\mathrm{m}$. The results obtained with the CVA shows a more symmetric profiles and a larger peak. This is attributed to the larger frequency response of the CVA that allows to capture the temperature fluctuations associated with the smaller scales. The standard deviation has a shape that can be modelled as bell shaped membership function

$$\frac{\sigma_T}{T_j - T_{amb}} = \frac{0.12}{1 + \left(\frac{\eta+\eta_0}{1.2}\right)^4} \tag{10}$$

where 0.12 is the maximum of the normalized temperature standard deviation found experimentally.

The different frequency response can be evidenced by reporting the temperature spectra obtained at the peak of the temperature standard deviation profile, shown in Fig. 2(b). The cut-off frequency of the CCA is in fact approximately equal to 900 Hz while it increases to 3000 Hz for the CVA. In the figure, the effect of the wire diameter on the cut-off frequency is reported. The CCA wire having the diameter of 1 μm over-perform the CCA having a larger diameter (2.5 μm) that was used in the current investigation for the sensitivity correction.

The lower frequency response of the CCA can explain the lack of the self similarity in the skewness as reported in Fig. 13. Similarly to the velocity skewness, the temperature skewness is positive towards the lower velocity/temperature and negative towards the high velocity/temperature region, namely the core of the jet.

3.5. Velocity–temperature correlation

Relying on the temperature fluctuations obtained with the CVA, θ, the streamwise turbulent heat flux correlation coefficient, $\overline{u\theta}$ is calculated. The profiles, normalized by the standard deviation of the velocity and the temperature in shown in Fig. 14. The values collapse when changing the streamwise location (not reported here) as well as the free-stream velocity. Despite the difference in the shape of the profiles with respect to the results by Ferchichi and Tavoularis (1992), who reported a Gaussian-like shape, while here a double peak profile can be highlighted, the peak value is similar and approximately equal to 0.6. This shows how there is large correlation between thermal and velocity fluctuations in the shear layer.

4. Concluding remarks and summary

We employed planar PIV and hot-wire anemometry to characterize the turbulent shear layer that naturally evolves from an initial laminar state due to the velocity differences between a jet and the surrounding quiescent region. In the portion of the turbulent shear layer under investigation, all hypotheses regarding its self-similarity were validated. Specifically, these include the collapse of statistics when plotted against reduced quantities, the plateau of statistics in the streamwise direction, and the linear growth of the turbulent shear layer.

The SPOD results reveal the presence of dominant large-scale coherent structures that span the entire transverse extent of the shear layer, consistent with observations from flow visualization by D'Ovidio and Coats (2013) and large-eddy simulations by McMullan et al. (2015). The first SPOD mode captures structures that account for approximately 30% of the total turbulent kinetic energy within the mixing layer, highlighting their energetic significance.

While these structures resemble the *flow cells* proposed by McMullan et al. (2015) that drive continuous growth in the post-transition regime, we refrain from making definitive claims about the underlying

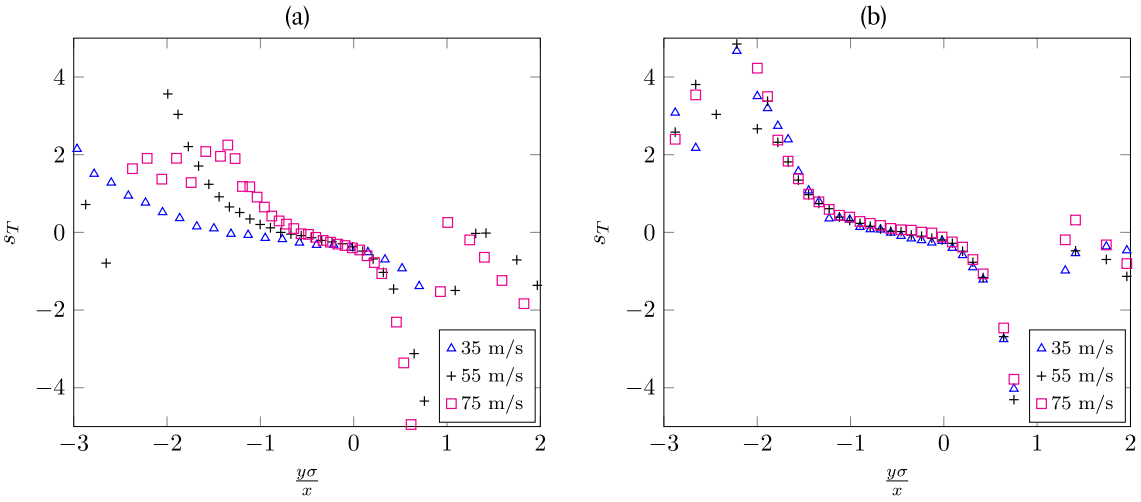

Fig. 13. Self similarity of the Skewness profile of the temperature, comparison CCA (a) and CVA (b) cold wire at $x = 0.5$ m.

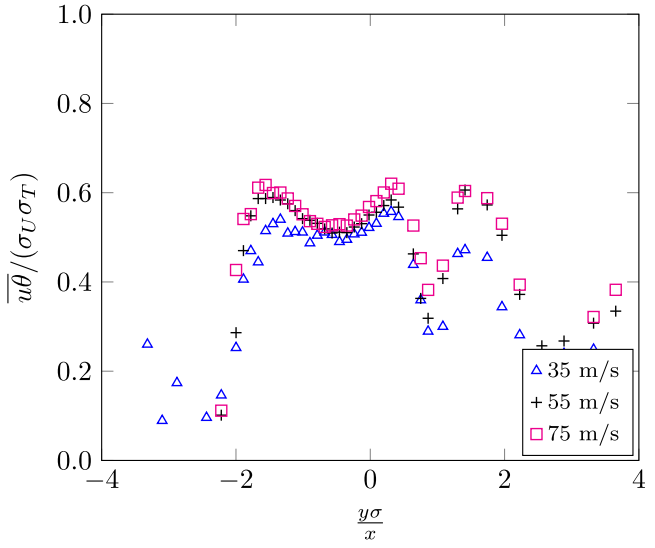

Fig. 14. Streamwise turbulence heat flux correlation coefficient, CVA cold wire correction for the velocity fluctuation and temperature fluctuation, effect of the free-stream velocity at $x = 0.5$ m.

growth mechanism. Interestingly, the dominant structures are associated with a Strouhal number of approximately 0.2, which is close to the characteristic frequency of Kelvin–Helmholtz instabilities typically observed in pre-transition shear layers. This similarity raises important questions about the nature of the growth process in post-transition regimes and suggests that, despite different underlying dynamics, some features of the pre-transition shear layer may remain robust. We further demonstrated that this frequency is not dissimilar with respect to the passage time of large structures. We estimated the spacing between the large structures obtaining a value of $4.3\delta_\omega$ which aligns with the relationship proposed by Browand and Troutt (1985), supporting the hypothesis by D'Ovidio and Coats (2013) of a consistent average spacing-to-thickness ratio.

Overall, our results contribute new experimental evidence to the ongoing discussion on coherent structure development in turbulent shear layers and underscore the need for further investigation with SPOD using experimental dataset where both temporal and three-dimensional dynamics are resolved.

The thermal shear layer was characterized using CCA and CVA cold wire measurements. The importance of employing a CVA cold wire for thermal characterization was highlighted, as it offers a higher frequency response compared to the CCA. We demonstrated that the thermal shear layer exhibits self-similarity when the normalization method proposed in this study is applied. The thermal shear layer displays a different growth rate compared to the velocity shear layer. Finally, new analytical formulations are introduced, providing universal non-dimensional profiles for the mean and standard deviation of temperature.

CRediT authorship contribution statement

Francesco Scarano: Writing – review & editing, Writing – original draft, Visualization, Methodology, Investigation, Formal analysis, Data curation, Conceptualization. **Emmanuel Jondeau:** Methodology, Investigation. **Édouard Salze:** Supervision, Resources, Project administration, Investigation.

Funding

The present study is part of the program MAMBO "Méthodes avancées pour la modélisation du bruit moteur et avion" (Advanced methods for engine and aicraft noise modelling), coordinated by Airbus SAS. It was supported by the Direction Générale de l'Aviation Civile (DGAC) under the Grant no 2021-50. This work was also performed within the framework of the Labex CeLyA of the Université de Lyon, within the programme Investissements dt'Avenir (ANR-10-LABX-0060/ANR-16-IDEX-0005) operated by the French National Research Agency

Declaration of competing interest

The authors declare that they have no known competing financial interests or personal relationships that could have appeared to influence the work reported in this paper.

Data availability

Data will be made available on request.

References

Bell, J.H., Mehta, R.D., 1990. Development of a two-stream mixing layer from tripped and untripped boundary layers. AIAA J. 28 (12), 2034–2042. http://dx.doi.org/10.2514/3.10519, URL https://arc.aiaa.org/doi/10.2514/3.10519.

Bennaceur, I., 2017. Etude Numérique de la Diffusion d'Une Onde Acoustique Par une Couche de Cisaillement Turbulente à l'Aide d'une Simulation aux Grandes Échelles (Ph.D. thesis). URL http://www.theses.fr/2017AIXM0187. Thèse de doctorat dirigée par Dupont, Pierre et Larchevêque, Lionel Sciences de l'ingénieur. Mécanique et physique des fluides Aix-Marseille 2017.

Berson, A., Poignand, G., Blanc-Benon, P., Comte-Bellot, G., 2010. Capture of instantaneous temperature in oscillating flows: Use of constant-voltage anemometry to correct the thermal lag of cold wires operated by constant-current anemometry. Rev. Sci. Instrum. 81 (1), 015102. http://dx.doi.org/10.1063/1.3274155, URL https://pubs.aip.org/rsi/article/81/1/015102/355689/Capture-of-instantaneous-temperature-in.

Browand, F.K., Troutt, T.R., 1985. The turbulent mixing layer: geometry of large vortices. J. Fluid Mech. 158, 489–509. http://dx.doi.org/10.1017/S0022112085002737, URL https://www.cambridge.org/core/product/identifier/S0022112085002737/type/journal_article.

Brown, G.L., Roshko, A., 1974. On density effects and large structure in turbulent mixing layers. J. Fluid Mech. 64 (4), 775–816. http://dx.doi.org/10.1017/S002211207400190X, URL https://www.cambridge.org/core/product/identifier/S002211207400190X/type/journal_article.

Candel, S., Guedel, A., Julienne, A., 1976a. Radiation, refraction and scattering of acoustic waves in a free shear flow. In: 3rd Aeroacoustics Conference. American Institute of Aeronautics and Astronautics, Palo Alto,CA,U.S.A., http://dx.doi.org/10.2514/6.1976-544, URL https://arc.aiaa.org/doi/10.2514/6.1976-544.

Candel, S., Julliand, M., Julienne, A., 1976b. Shielding and scattering by a jet flow. In: 3rd Aeroacoustics Conference. American Institute of Aeronautics and Astronautics, Palo Alto,CA,U.S.A., http://dx.doi.org/10.2514/6.1976-545, URL https://arc.aiaa.org/doi/10.2514/6.1976-545.

Carlier, J., Sodjavi, K., 2016. Turbulent mixing and entrainment in a stratified horizontal plane shear layer: joint velocity2013temperature analysis of experimental data. J. Fluid Mech. 806, 542–579. http://dx.doi.org/10.1017/jfm.2016.592.

Cleve, S., Jondeau, E., Blanc-Benon, P., Comte-Bellot, G., 2017. Cold wire constant voltage anemometry to measure temperature fluctuations and its application in a thermoacoustic system. Rev. Sci. Instrum. 88 (4), 044904. http://dx.doi.org/10.1063/1.4979823, URL https://pubs.aip.org/rsi/article/88/4/044904/357324/Cold-wire-constant-voltage-anemometry-to-measure.

D'Ovidio, A., Coats, C.M., 2013. Organized large structure in the post-transition mixing layer. Part 1. Experimental evidence. J. Fluid Mech. 737, 466–498. http://dx.doi.org/10.1017/jfm.2013.553, URL https://www.cambridge.org/core/product/identifier/S0022112013005533/type/journal_article.

Ferchichi, M., Tavoularis, S., 1992. Evolution of a thermal mixing layer in uniformly sheared turbulent flow. Phys. Fluids A: Fluid Dyn. 4 (5), 997–1006. http://dx.doi.org/10.1063/1.858226, URL https://pubs.aip.org/pof/article/4/5/997/402696/Evolution-of-a-thermal-mixing-layer-in-uniformly.

Gautam, A., Livescu, D., Mejia-Alvarez, R., 2024. Growth of organized flow coherent motions within a single-stream shear layer: 4D-PTV measurements. Exp. Fluids 65, http://dx.doi.org/10.1007/s00348-024-03846-5.

Gortler, H., 1942. Berechnung von aufgaben der freien turbulenz auf grund eines neuen näherungsansatzes. ZAMM - Z. Angew. Math. Mech. 22 (5), 244–254. http://dx.doi.org/10.1002/zamm.19420220503, URL https://onlinelibrary.wiley.com/doi/10.1002/zamm.19420220503.

McMullan, W.A., Gao, S., Coats, C.M., 2015. Organised large structure in the post-transition mixing layer. Part 2. Large-eddy simulation. J. Fluid Mech. 762, 302–343. http://dx.doi.org/10.1017/jfm.2014.660, URL https://www.cambridge.org/core/product/identifier/S0022112014006600/type/journal_article.

Mercier, B., Jondeau, E., Castelain, T., Ozawa, Y., Bailly, C., Comte-Bellot, G., 2019. High frequency temperature fluctuation measurements by Rayleigh scattering and constant-voltage cold-wire techniques. Exp. Fluids 60 (7), 110. http://dx.doi.org/10.1007/s00348-019-2753-y, URL http://link.springer.com/10.1007/s00348-019-2753-y.

Michaelis, D., Neal, D.R., Wieneke, B., 2016. Peak-locking reduction for particle image velocimetry. Meas. Sci. Technol. 27 (10), 104005. http://dx.doi.org/10.1088/0957-0233/27/10/104005, URL https://iopscience.iop.org/article/10.1088/0957-0233/27/10/104005.

Michalke, A., 1965. Vortex formation in a free boundary layer according to stability theory. J. Fluid Mech. 22 (2), 371–383. http://dx.doi.org/10.1017/S0022112065000812.

Mohammed-Taifour, A., Weiss, J., Sadeghi, A., Vétel, J., Jondeau, E., Comte-Bellot, G., 2015. A detailed procedure for measuring turbulent velocity fluctuations using constant-voltage anemometry. Exp. Fluids 56 (9), 174. http://dx.doi.org/10.1007/s00348-015-2045-0, URL http://link.springer.com/10.1007/s00348-015-2045-0.

Perry, A., 1982. Hot-Wire Anemometry. Oxford University Press.

Rogers, M.M., Moser, R.D., 1994. Direct simulation of a self-similar turbulent mixing layer. Phys. Fluids 6 (2), 903–923. http://dx.doi.org/10.1063/1.868325, URL https://pubs.aip.org/pof/article/6/2/903/420452/Direct-simulation-of-a-self-similar-turbulent.

Scarano, F., Jondeau, E., Salze, E., 2024. A simple hot wire temperature drift correction based on temperature sensitivity applied to a turbulent shear layer. Phys. Fluids 36 (10), 105192. http://dx.doi.org/10.1063/5.0232138, _eprint: https://pubs.aip.org/aip/pof/article-pdf/doi/10.1063/5.0232138/20225699/105192_1_5.0232138.pdf.

Schmidt, O.T., Colonius, T., 2020. Guide to spectral proper orthogonal decomposition. AIAA J. 58 (3), 1023–1033. http://dx.doi.org/10.2514/1.J058809, URL https://arc.aiaa.org/doi/10.2514/1.J058809.

Sciacchitano, A., 2019. Uncertainty quantification in particle image velocimetry. Meas. Sci. Technol. 30, http://dx.doi.org/10.1088/1361-6501/ab1db8.

Suryanarayanan, S., Narasimha, R., 2017. Insights into the growth rate of spatially evolving plane turbulent free-shear layers from 2D vortex-gas simulations. Phys. Fluids 29 (2), 020708. http://dx.doi.org/10.1063/1.4974516, arXiv:https://pubs.aip.org/aip/pof/article-pdf/doi/10.1063/1.4974516/14937110/020708_1_online.pdf.

Towne, A., Schmidt, O.T., Colonius, T., 2018. Spectral proper orthogonal decomposition and its relationship to dynamic mode decomposition and resolvent analysis. J. Fluid Mech. 847, 821–867. http://dx.doi.org/10.1017/jfm.2018.283, URL https://www.cambridge.org/core/product/identifier/S0022112018002835/type/journal_article.

Townsend, A., 1976. The Structure of Turbulent Shear Flow. Cambridge University Press.

Tropea, C., Yarin, A., Foss, J., 2007. Springer handbook of experimental fluid mechanics. pp. 229–287. http://dx.doi.org/10.1007/978-3-540-30299-5.

Winant, C.D., Browand, F.K., 1974. Vortex pairing: the mechanism of turbulent mixing-layer growth at moderate Reynolds number. J. Fluid Mech. 63 (2), 237–255. http://dx.doi.org/10.1017/S0022112074001121.